GENETICS, 2022, 221(3), iyac076
https://doi.org/10.1093/genetics/iyac076
Advance Access Publication Date: 10 May 2022
Investigation

A network modeling approach provides insights into the environment-specific yield architecture of wheat

Noah DeWitt [1,2,*] Mohammed Guedira,[1] Joseph Paul Murphy,[1] David Marshall,[2] Mohamed Mergoum,[3] Christian Maltecca [4] and Gina Brown-Guedira [1,2]

[1]Department of Crop and Soil Sciences, North Carolina State University, Raleigh, NC 27695, USA,
[2]Plant Science Research, USDA-ARS SEA, Raleigh, NC 27695, USA,
[3]Department of Crop and Soil Sciences, University of Georgia, Athens, GA 30602, USA,
[4]Department of Animal Science, North Carolina State University, Raleigh, NC 27695, USA

*Corresponding author: Department of Crop and Soil Sciences, North Carolina State University, Raleigh, NC 27695, USA. Email: noah.dewitt@usda.gov

Abstract

Wheat (*Triticum aestivum*) yield is impacted by a diversity of developmental processes which interact with the environment during plant growth. This complex genetic architecture complicates identifying quantitative trait loci that can be used to improve yield. Trait data collected on individual processes or components of yield have simpler genetic bases and can be used to model how quantitative trait loci generate yield variation. The objectives of this experiment were to identify quantitative trait loci affecting spike yield, evaluate how their effects on spike yield proceed from effects on component phenotypes, and to understand how the genetic basis of spike yield variation changes between environments. A 358 $F_{5:6}$ recombinant inbred line population developed from the cross of LA-95135 and SS-MPV-57 was evaluated in 2 replications at 5 locations over the 2018 and 2019 seasons. The parents were 2 soft red winter wheat cultivars differing in flowering, plant height, and yield component characters. Data on yield components and plant growth were used to assemble a structural equation model to characterize the relationships between quantitative trait loci, yield components, and overall spike yield. The effects of major quantitative trait loci on spike yield varied by environment, and their effects on total spike yield were proportionally smaller than their effects on component traits. This typically resulted from contrasting effects on component traits, where an increase in traits associated with kernel number was generally associated with a decrease in traits related to kernel size. In all, the complete set of identified quantitative trait loci was sufficient to explain most of the spike yield variation observed within each environment. Still, the relative importance of individual quantitative trait loci varied dramatically. Path analysis based on coefficients estimated through structural equation model demonstrated that these variations in effects resulted from both different effects of quantitative trait loci on phenotypes and environment-by-environment differences in the effects of phenotypes on one another, providing a conceptual model for yield genotype-by-environment interactions in wheat.

Keywords: yield components; structural equation modeling; QTL mapping; yield variation

Introduction

Wheat breeders have increased grain yield and stability by selecting for greater yield potential, despite little understanding of the genetic basis of that potential. Breeders and geneticists have successfully characterized the genetic basis of disease resistance and used marker-assisted selection (MAS) to deploy resistance in new cultivars, but the characterization and use of beneficial variants for yield potential have been less successful. One approach to disentangle the complexity of grain yield is to break it down into component traits (Grafius 1964; Brinton and Uauy 2019). In this view, per-acre wheat yield is a product of the number of spikes per square meter and spike yield (SY), which can be thought of as the product of kernel number per spike (KN) and thousand kernel weight (TKW) (Fig. 1). TKW can be further decomposed into kernel area (KA), kernel width (KW), kernel length (KL), and kernel density. Kernel number per spike depends on the number of spikelets per spike (SpS), and the mean number of kernels per spikelet (KpS, related to floret fertility). Increased kernel number, rather than kernel weight, has driven increased wheat yield (Fischer 2008). Researchers understand that plants typically compensate for an increase in kernel number through a decrease in kernel size and vice versa, but the extent to which this is driven by pleiotropy or physiology is unclear (Knott and Talukdar 1971). Loci with positive impacts on grain size with no kernel number tradeoff exist, suggesting it is possible to improve yield by identifying yield component QTL (Sadras 2007; Griffiths *et al.* 2015). Evidence that most modern wheat cultivars are sink-limited (Borrás *et al.* 2004), suggests that negative correlations between grain size and number may result from the mechanisms of underlying genes rather than resource constraints.

Selecting for increases in sink tissue is therefore a promising strategy for increasing yield. Mapping and cloning of the major variants influencing floral and grain morphology may facilitate prediction through MAS and improved GS models, but

Received: April 08, 2022. **Accepted:** May 01, 2022
Published by Oxford University Press on behalf of Genetics Society of America 2022.

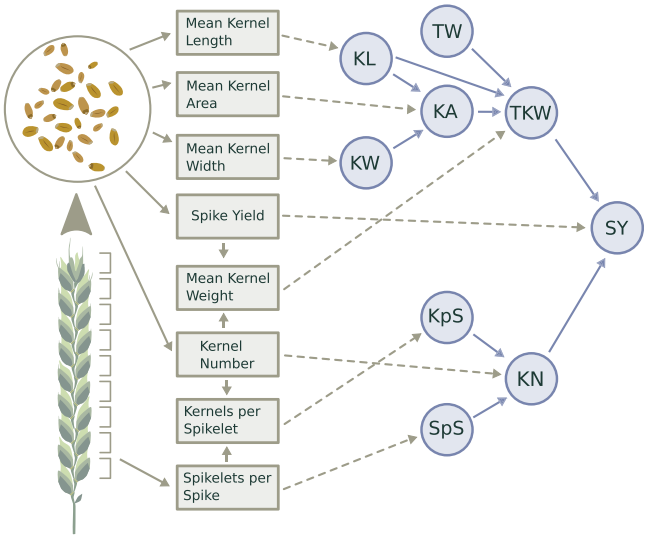

Fig. 1. Phenotyping of yield component traits in the LM population. The figure represents the full set of yield component phenotypes collected at the Raleigh NC (RAL19), Kinston NC (KIN19), and Plains GA (GA19) locations in 2019, excluding test weight (TW). Collected traits relate to the phenotypes within the conceptual yield component model, where phenotypes are taken to be the product of component phenotypes, such that SY = TKW × KN, TKW = TW × KW × KA, and so on. Some collected phenotypes are used to calculate other yield components, represented by arrows linking tan boxes.

importantly should provide insight into the biology underlying phenotypic variation. The development of genomic resources in the wheat community has led to the mapping and cloning of well-studied wheat alleles with large effects on floral and grain morphology, including super-domestication gene *Q* controlling the spelt character (Simons *et al.* 2006), *S* controlling the semi-dwarf and spherical grain characters of *sphaerococcum* wheat (Cheng *et al.* 2020), and *B1* controlling the awnless character in most germplasm (DeWitt *et al.* 2020). More recently, new variants affecting yield components have been identified and cloned; *TaGW-A2* has been characterized as a functional variant in a negative regulator of grain weight (Su *et al.* 2011; Wang *et al.* 2018), while a major variant in floral developmental gene *WAPO-A1* increases the number of spikelets per spike (Kuzay *et al.* 2019).

Variation in plant growth also impacts yield and its components. Major genes have been identified that control adult plant height (PH) and heading date. The physiological effect of the *Rht* genes, mutations in DELLA proteins that greatly reduce PH, is conditional on the environment and the quantity of assimilate produced by the cultivar. *RhtD1* is associated with larger kernel number but smaller kernel size and weight (Borner *et al.* 1993), a trade-off related not to spike development but to the greater availability of assimilates during grain-fill due to partitioning less biomass into stems (Youssefian *et al.* 1992). Semi-dwarf wheat cultivars having either the *Rht-D1b* or *Rht-B1a* allele are widely cultivated, as breeders generally select plants near some optimal height, because too-short plants have a generally lower yield (Fischer and Quail 1990) and tall plants tend to lodge. Variation for heading date generated by major-effect variants underlies the broad geographic distribution of cultivated wheat. Heading date variation alters the duration plants spend in certain developmental stages, which can impact developmental traits like kernel size and spikelet number per spike (Vargas *et al.* 2007). Plants with a mean heading date outside of the optimal range for a specific environment may expose themselves to early-season cold stress, late-season heat stress, or drought stress at sensitive developmental stages. Previous studies have demonstrated major effects of *Vrn1* and *Ppd1* alleles on final grain yield, often in an environment-specific manner related to climatic conditions (Addison *et al.* 2016, unpublished results). A variant may have a large effect on a single plant growth phenotype that will translate into a smaller effect on yield component traits and, in turn, to yield variation. For example, the insensitive allele at the major heading date gene *Ppd-D1*, alters expression of intermediates that upregulate other genes in the flowering time pathway, hastening the development of the shoot apical meristem which in turn reduces the number of spikelets per head (Boden *et al.* 2015). Decreases in spikelet number may decrease SY, depending on the relationships between yield components in a given environment. Variation for these developmental traits then alters yield in an environment-specific manner. Using QTL for the improvement of yield requires an understanding of how those QTL alter yield. A "yield QTL" useful for MAS should alter yield components in a way that consistently produces an increase in yield in the targeted environment without altering plant growth over time.

The structural equation modeling (SEM) framework fits multivariate data to a network structure that links variables via effects. Path analysis and SEM have been used in a variety of fields (e.g. Wright 1920; Crespi and Bookstein 1989; Kaplan and Phillips 2006). In the context of crop genetics, they can model the translation of sequence variation into yield variation through intermediate phenotypes. SEM has been recently used to increase the power of GWAS by incorporating information on multiple correlated traits (Momen *et al.* 2018, 2019). In wheat, SEM has been used within chromosome substitution lines to identify QTL for yield via effects on grain number and weight (Dhungana *et al.* 2007; Mi *et al.* 2010). At the same time, SEM has been used to show the importance of variation in plant growth traits in generating variation in seed number, size, and yield in small numbers of genotypes (Vargas *et al.* 2007). We chose to apply SEM in this study because, unlike standard multitrait models that assume direct effects of QTL on all traits, SEM allows linking QTL to SY via a graph of intermediate phenotypes with a known structure to understand the basis of changes in QTL effects on SY between environments.

In DeWitt *et al.* (2021), we characterized the genetic basis of heading date and PH in the LA-95135×SS-MPV-57 biparental recombinant inbred line (RIL) population. These traits follow an oligogenic architecture, with over 90% of additive genetic variation for heading date and PH associated with 6 QTLs in most environments. Here, we build off this prior work to understand the relationship between these QTL and yield, characterize new QTL that are associated with yield component traits but not heading date or PH, and understand the basis of their contribution to SY variation in an environment-specific manner.

Materials and methods

Population development and phenotyping

A RIL population developed from a cross between cultivars SS-MPV-57 (FFR555W/3/VA89-22-52/TYLER//REDCOAT*2/GAINES) and LA-95135 (CL-850643/PIONEER-2548//COKER-9877/3/FLORIDA-302/COKER-762) was used in this study. The parents of the population were chosen to generate major additive genetic variation for PH and flowering time and to characterize novel QTL for these traits. Parent SS-MPV-57 carries major earliness gene *Ppd-D1a*, but no major dwarfing genes, and parent LA-95135 caries major dwarfing gene *Rht-D1b*, but no major earliness genes. At the same time, recently

cloned major variants *WAPO-A1*, *TaGW-A2*, and *B-A1* (Supplementary Table 1) segregate in this population, allowing for the investigation of their effects on different yield components in a common background (Su *et al.* 2011; Wang *et al.* 2018; Kuzay *et al.* 2019; DeWitt *et al.* 2020). After crossing, F_1 plants were selfed to generate a population of F_2 lines. Plants were advanced via the single-seed descent method until the F_5 generation, producing 360 RILs.

The LA-95135×SS-MPV-57 RIL population (hereafter referred to as the LM population) was evaluated in the field at Raleigh, NC (RAL18) and Kinston, NC (KIN18) during the 2018 field season, and in 2019 at Raleigh (RAL19), Kinston (KIN19), and Plains, GA (GA19). Despite being located 70 miles away, Raleigh and Kinston tend to be distinct environments separated by the Atlantic Seaboard fall line. Raleigh falls within the North American Piedmont environment characterized by higher elevations and clay soils, while Kinston is a warmer environment on the Atlantic coastal plain with generally sandier and loamier soils (Supplementary Table 2). Lines head earlier and experience greater biotic and abiotic stress in Kinston relative to Raleigh. Plains is located in the southern part of the Atlantic coastal plain, and lines typically head much earlier, experience greater heat and drought stress during grain fill, and see high levels of rust pathogens. The 360 RILs were grown in an augmented block experiment with 3 replications of the parents per block, and 2 replications of each RIL at each location. Each of the 5 blocks consisted of 72 RIL entries, and plots consisted of 1-m rows spaced 30 cm apart. PH was collected as the height of the top of the spikes, excluding the awns, of a sample of tillers from the center of each row. Heading date of each row was noted as the day of year when half of the heads had fully emerged from the flag leaf, typically a few days before anthesis.

Grain yield in this study is treated as the product of kernel number and size (Fig. 1). Kernel size was collected as TKW and kernel size components (kernel length, KL; kernel width, KW), while SpS and KpS were collected as components of kernel number. Six representative spikes from each row were harvested and number of spikelets recorded for all field experiments. Seeds were weighed and counted to determine kernel weight. Rows at the RAL18 location were hand harvested and threshed using a Vogel thresher. A 15-ml seed sample was cleaned and grain morphometric parameters (kernel length, width, area, and weight) were obtained using a MARVIN grain analyzer (GAT Sensorik GMBH, Neubrandenburg, Germany). Kernel morphometric parameters and total SY for the KIN18 experiment and all 2019 field experiments were obtained by sampling seed threshed from the 6-spike sample of each row using a scale and a Vibe QM3 grain analyzer (Vibe Image Analytics Ltd., Capitola, CA). In all locations, SpS was calculated as the mean number of fertile spikelets on the sampled wheat spikes.

Analysis of phenotypes

For QTL mapping, values for each genotype were calculated for each combination of phenotype and environment as best linear unbiased estimates (BLUEs). To correct for effects related to plants' physical positions within a field, the software Echidna (Gilmour 2018) was used to calculate BLUEs with an AR1xAR1 spatial adjustment model:

$$y_i \sim \mu + G_i + u_i + e_i,$$

where y_i is the observed phenotype for an individual row, μ is the intercept, G_i is the fixed effect of genotype, and u_i is the unit or "nugget" random effect for each observation representing the component of the variance associated with sampling or other uncorrelated error drawn from a distribution $u \sim iid\mathcal{N}(0, \sigma_e^2)$, and e_i is the spatially correlated residual drawn from an AR1xAR1 residual structure (see Gilmour *et al.* 1997). While the unit variance is modeled as a random effect it is really a residual; the AR1xAR1 residual variance structure absorbs correlated error associated with physical positions of plots (e.g. poor locations in the field that decrease phenotype values in closely positioned plots), while the unit variance represents uncorrelated errors associated with individual plots or measurement plots (e.g. human error in counting SpS) (Isik *et al.* 2017). For SEM, phenotypes were centered and scaled to a mean of 0 and SD of 1.

Network modeling

The structure of the conceptual yield component model (Fig. 1) was extended to estimate allele effects of QTL on SY as the product of effects on component phenotypes by fitting a SEM using the R package lavaan (Fig. 2). In this model, a QTL effect on SY is the sum of the products of effects on the base yield components (KL, KW, KpS, SpS, and TKW) and the mediated effects of the QTL on downstream phenotypes via the base phenotypes. Correlation coefficients between linked variables are taken as causal effects of variables on other variables using prior knowledge of the relationships between phenotypes. This model was extended with information on phenotypes that may affect yield components—PH, heading date, and leaf rust severity—to generate a graph relating QTL affecting these traits to SY through a set of intermediate phenotypes (Fig. 2). In all cases, effects were estimated for the allele inherited from the LA-95135 parent.

The effects of QTL on traits and the effect of traits on each other were estimated by fitting the graph in each environment in lavaan. In the case of a multivariate SEM without latent variables, the simple matrix form is $\mathbf{Y} = \mathbf{\Lambda}Y + \mathbf{e}$, where $\mathbf{Y}$ is a matrix of n phenotypes, and $\mathbf{\Lambda}$ is an nxn lower-triangular matrix where cells representing relationships between values are either 0, representing no relationship between variables, or a coefficient that estimates the effect of one variable on another. Yield component traits were allowed to have effects on the other yield components that were set later in plant development (e.g. altered values of SpS can affect KL, but not vice versa). The total allele effect of a QTL on SY was calculated using path analysis, multiplying the effects of the QTL on associated phenotypes by the effects of those phenotypes on subsequent phenotypes, and summing all paths.

QTL mapping

Genotypic data were obtained from a combination of genome wide markers derived from genotype-by-sequencing (GBS) and markers for known polymorphisms assayed with Kompetitive Allele-Specific Primer (KASP) markers. Both GBS and KASP markers were used to construct a linkage map for the LM population as described in DeWitt *et al.* (2021). Two RILs with a high proportion of missing GBS data were excluded from subsequent analyses to produce a final RIL population of 358 lines QTL mapping of PH and heading date genes was performed as described previously using the R package r/QTL (Broman *et al.* 2003). Initial data collected in 2018 comprised a more limited set of yield components, specifically TKW and SpS. Univariate QTL analyses were conducted for these traits in these 2 environments, to contrast with the alternate multivariate SEM approach conducted with the more complete set of phenotypes collected in 2019. For initial univariate QTL identification for SpS and TKW data collected in 2018, composite interval mapping was used for preliminary

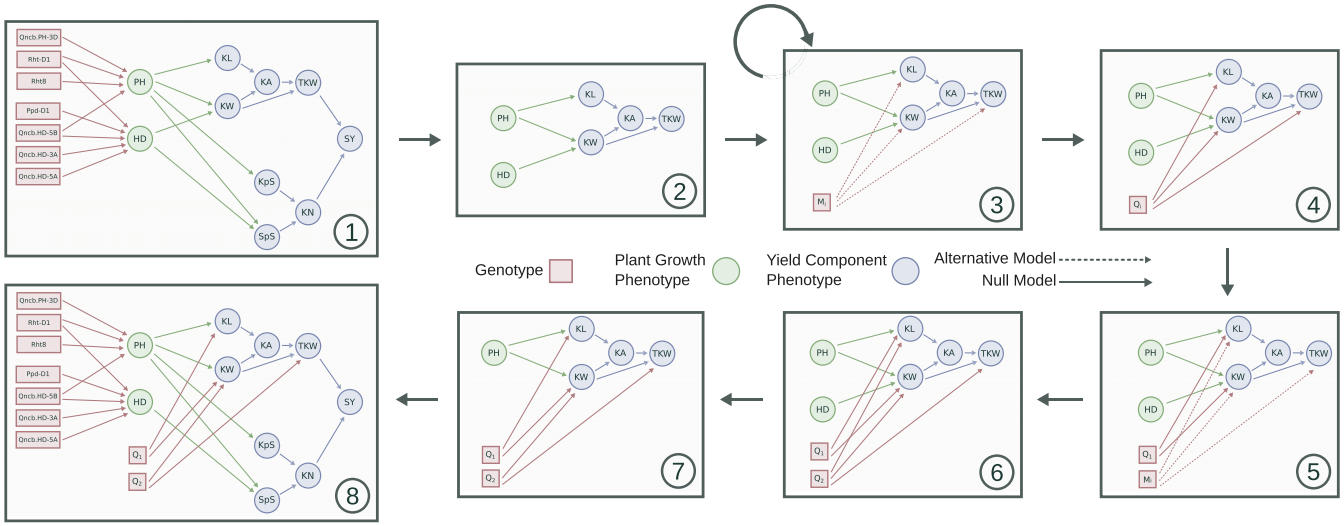

Fig. 2. SEM QTL mapping model steps in the QTL mapping model, where dashed lines represent tested genome-wide markers. The iteration for QTL having effects on TKW, KL, and KW is shown. A full description of the model is given in the *QTL Mapping* section.

identification of major QTL, and intervals were narrowed using a multiple QTL model (MQM) as implemented in the *refineqtl()* function. The *addqtl()* function was used to identify additional QTL using identified QTL as covariates, without testing for non-additive interactions between mapped QTL. Genome-wide significance thresholds for an $\alpha = 0.05$ were determined in r/QTL by performing QTL scans for 1,000 random genotype permutations through the function *scanone()*.

Given the degree of correlation between our phenotypes, most identified yield QTL are expected to have pleiotropic effects on more than one yield component trait. Thus, a multivariate model that included components was expected to have more power to detect a QTL for SY than a traditional QTL model. In addition, to identify yield component QTL that are not heading date or PH QTL with mediated effects on yield components, those phenotypes should be considered as covariates in the analysis. We implemented a network mapping approach to account for the observation that each specific QTL does not have pleiotropic effects on all phenotypes, but affect different subsets of traits. To model the existence of "per se" yield component QTL the effect of markers in a network model was tested directly using the following steps:

1) Specify a prior graph featuring effects of known genes on phenotypes, and relationships between phenotypes (Fig. 2, panel 1).
2) Test each combination of base yield component phenotypes, starting with the maximal case of all 5, and moving to subsets of phenotypes. Iterations with reduced phenotypes test for QTL that have overall significant effects on 4 or less phenotypes.
3) For each set of phenotypes, consider all relevant variables affecting those phenotypes (Fig. 2, panel 2).
4) Generate 1,000 random permutations of the genotype data (Fig. 2, panel 3). For each permutation:
   a) For each permuted marker, compute the log likelihood of the null model of no effect of the tested marker on the base yield components using the *sem()* function in lavaan. Compute the likelihood of the alternative model of an effect of the tested marker on the base yield components, and take the difference as a log of odds (LOD) score.
   b) Return the LOD value of the permuted marker with the largest LOD score as representing the iteration.
   c) Order the vector of maximum LOD values and take the 95th percentile value as a conservative empirical significance threshold at α=0.05.
   d) For each nonpermuted marker, compute and compare the likelihoods of alternative and null models using the sem() function in lavaan. Genome-wide markers are tested individually to identify the most significant marker and compare it to the significance threshold. Take the model with the highest LOD score as an updated model for that set of phenotypes (Fig. 4, panel 4).
   e) Refit the model with the added marker and remove any nonsignificant paths between the new marker and phenotypes (Fig. 2, panel 5)
   f) Remove any other paths that have become nonsignificant because of addition of new variables.
5) Repeat steps a–f until no further markers pass the LOD threshold (Fig. 2, panels 6 and 7).
6) Replace the sections of the full graph considered in the current iteration with the updated subgraph containing any new QTL and their relationships to phenotypes (Fig. 2, panel 8).

Genotype permutations were performed with the *sim.geno()* function in r/QTL. Number of identified yield component QTL used in significance threshold testing was limited to 8 to prevent over-fitting of the model and maintain a conservative significance threshold, and mapped QTL within 2 cM of an existing QTL were treated as the same QTL affecting different phenotypes. The procedure was repeated separately for each environment. In the Plains 2019 environment where PH was not collected, PH was modeled as a latent variable measured by the PH variables collected in the other 4 environments. The final model for each environment was fit using the *sem()* function in lavaan to estimate

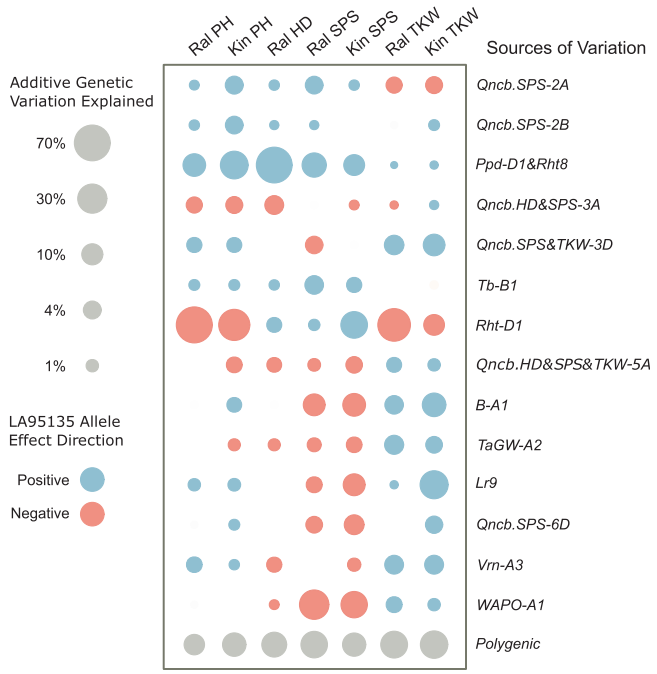

Fig. 3. Additive genetic variation associated with yield component QTL. Additive genetic variation for phenotypes collected in Raleigh and Kinstson in the 2018 field season (PH, plant height; HD, heading date; SpS, spikelets-per-spike; TKW, thousand kernel weight) is partitioned into components associated with mapped SpS and TKW QTL and all other QTL (polygenic effect). QTL that have a positive effect on SpS generally have a negative effect on TKW, and vice versa.

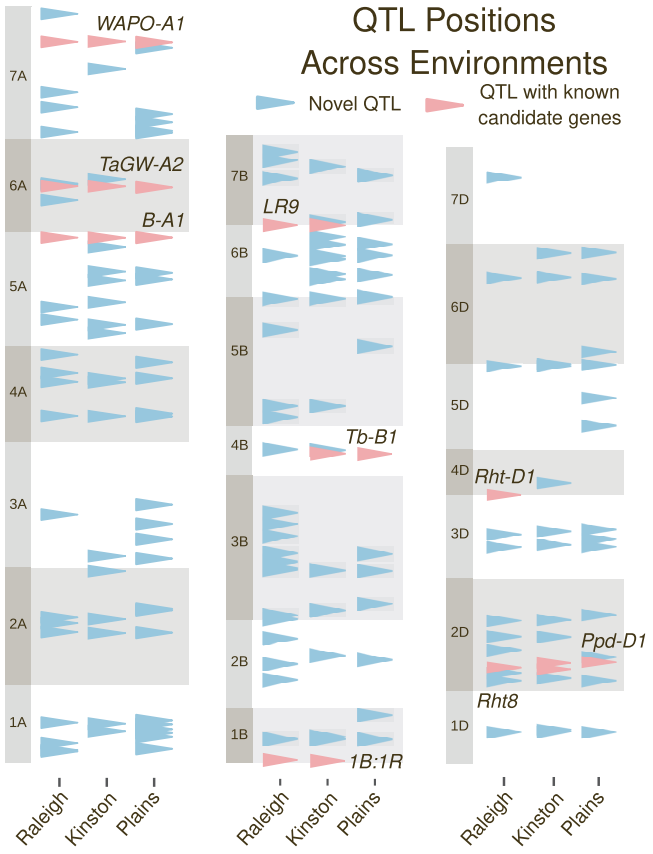

Fig. 4. Mapped QTL across locations QTL added to the model for any combination of traits, plotted by genetic position across all 3 subgenomes in each of three 2019 environments (Raleigh 2019, RAL19; Kinston 2019, KIN19; Plains 2019, GA19). The name of known genes associated with mapped QTL are noted.

coefficients for path analysis of the effects of individual QTL on SY and its components.

Variance, path analysis, and prediction

To assess the relative importance of mapped QTL in generating additive genetic variation in collected phenotypes, variance analysis was performed in the R package lme4qtl, which allows for the fitting of random effects with supplied covariance matrices (Ziyatdinov *et al.* 2018). For known variants for which KASP marker genotypes of the causal polymorphisms were available, the genotypes were used directly, and for novel QTL genotype probabilities from the refineqtl object were used. For testing QTL, alleles were encoded in terms of the allele dosage of the LA-95135 allele (0, 1, 2) without estimating a dominance effect.

For each environment and phenotype, QTL effects and variance components for both the additive and nonadditive effects of genotypes were specified with the mixed model:

$$y_{ik} \sim \sum_{h=1}^{n} Q_{ih} + g_{Ai} + g_{Ii} + e_{ik},$$

where for each phenotype Y of genotype i in row k, fixed effects for each QTL h were fit as regressions of allele dosage on phenotypes. The term g_{Ai} represents the random additive effect of genotype i with a variance specified by the realized relationship matrix ($g_A \sim \mathcal{N}(0, \mathbf{G}\sigma_g^2)$), calculated from the scaled GBS marker matrix ($\mathbf{G} = \frac{\mathbf{W}'\mathbf{W}}{c}$, where $\mathbf{W}$ is the scaled marker matrix and c is a normalization value calculated from allele frequencies of the markers). The term g_{Ii} represents the nonadditive random effect of genotype i with an independent variance ($g_I \sim \mathcal{N}(0, I\sigma_g^2)$).

A modified method from Nakagawa and Schielzeth (2013) used in DeWitt *et al.* (2021) was used to estimate variances associated with QTL and variance components from the specified model. The phenotypic variance absorbed by fixed effects in a mixed linear model was estimated as a function of QTL effect sizes and frequencies by multiplying the vector of values for an effect by its estimated effects and taking the variance of the vector ($\sigma^2_{\text{fixed}} = \text{Var}(\sum_{h=1}^{n} \beta_h x_{hk})$ for coefficients and effects h and observations k). Linked QTL *Ppd-D1* and *Rht8* were treated as a single locus to satisfy assumptions of independence between variables, using the mean genotype probabilities of the 2 QTLs.

The above model was modified to estimate variance components of SY by collectively estimating 2 additional random genotype effects associated with yield components and plant growth (heading date and PH) QTL. Relationship matrices were calculated as above except that genotypes for PH and heading date QTL were used to calculate a relationship matrix to estimate the variance associated with plant growth QTL, and genotypes for yield component traits identified using the SEM model were used to calculate a relationship matrix to estimate variance associated with yield component QTL. To verify that this model was appropriately partitioning variation, 100 iterations of a null model were run in which the same number of randomly sampled genome-wide SNP were used to construct the plant growth and yield component relationship matrices.

To assess the importance of mapped QTL in improving prediction accuracy for SY, a series of 3 models were run within each environment with 100 iterations of 5-fold cross-validation. As a baseline, a standard GBLUP model utilizing genotype data for all markers was fit as $y \sim \mu + u + e$, where y is a vector of BLUEs

Table 1. Significant yield component QTL information from best environment.

SpS: Chr.	Gene	Peak marker	Position CI	LOD	2α (SpS)	Sig. environments	Additional traits
2A		S2A_223722835	79–661 Mb	5.89	0.52	1	
2B		S2B_612673903	147–654 Mb	3.88	0.43	1	
2D	*Ppd-D1*	*Ppd-D1*	32–44 Mb	15.07	0.92	2	HD
3A		S3A_609909640	485–621 Mb	4.64	−0.48	1	HD
3D		S3D_476608044	434–549 Mb	3.58	−0.41	1	PH, TKW
4B	*Tb-B1*	S4B_416305737	52–620 Mb	3.71	0.41	1	
4D	*Rht-D1*	*Rht-D1*	0–35 Mb	12.1	0.96	1	PH, HD, TKW
5A.1		S5A_480804629	480–494 Mb	8.62	−0.74	2	HD, TKW
5A.2	*B-A1*	*B1*	698–703 Mb	12.9	−0.81	2	TKW
6B	*LR9*	*LR9*	701–721 Mb	6.45	−0.75	1	TKW
6D		S6D_250410640	55–323 Mb	4.22	−0.51	1	
7A	*WAPO-A1*	S7A_673096342	672–675 Mb	23.46	−1.10	2	
TKW: Chr.	**Gene**	**Peak marker**	**Position CI**	**LOD**	**2α(g)**	**Sig. environments**	**Additional traits**
3D		S3D_496955493	477–530 Mb	3.58	2.25	2	PH, SpS
4D	*Rht-D1*	*Rht-D1*	0–35 Mb	37.76	−5.52	2	PH, HD, SpS
5A.1		S5A_439551041	331–455 Mb	6.77	1.77	1	HD, SpS
5A.2	*B-A1*	*B1*	698–702 Mb	5.59	1.60	2	SpS
6A	*TaGW-A2*	S6A_355433083	97–509 Mb	5.81	1.66	1	
6B	*LR9*	*LR9*	701–721 Mb	11.42	2.40	1	SpS
7A.1	*VRN-A3*	S7A_66220298	58–77 Mb	4.75	1.48	1	HD
7A.2		S7A_149426090	128–516 Mb	5.51	1.61	1	

Data on TKW and SpS were collected in Raleigh and Kinston in 2018. For QTL significant in 2 environments, the effects, LOD score, and confidence interval from the most significant environment are displayed. Permutation testing-derived genome-wide significance thresholds for all traits were at or near a LOD of 3.50. QTL effects are given as twice the allele effect of the LA-95135 parent in the most significant environment (2α) for comparison of the effect between homozygous RILs. QTL for other phenotypes mapped near the confidence interval for a trait are given. Many QTL are mapped in the same regions as QTL for plant height (PH) and heading date (HD). QTLs mapped in the same region for both SpS and TKW tend to increase one while decreasing the other.

within each environment, μ is the overall mean, and u is a vector of genotype effects constrained by the genomic relationship matrix $\mathbf{G}$ as $u \sim \mathcal{N}(0, \mathbf{G}\sigma_u^2)$. Bayesian LASSO models were fit for both the full set of markers and the reduced set of mapped QTL, in both cases following the general model $\mathbf{y} = \mathbf{Xu} + \mathbf{e}$, where $\mathbf{X}$ is a marker matrix containing allele dosage of the LA-95135 allele, and vector of marker effects $\mathbf{u}$ is assumed to follow a double exponential prior distribution that accommodates a greater proportion of both large and near-zero marker effects. In both the full and reduced LASSO models, genotype values are calculated as the sum of marker effects $\hat{Y}_i = \sum_{j=1}^{n} x_{ij}\hat{u}_j$, where $\hat{u}_j$ is the estimated effect of marker j and x_{ij} is its dosage in individual i.

Results and discussion

Initial QTL identification

To investigate the genetic architecture of SpS and TKW in this population, single-trait QTL mapping was performed in the RAL18 and KIN18 environments. Twelve QTL were significantly associated (LOD > 3.54) with SpS, and 8 QTLs were significantly associated (LOD > 3.46) with TKW. Based on peak markers and confidence intervals, multiple QTL (Table 1) colocated with loci that were previously determined to affect PH and heading date in the population (DeWitt *et al.* 2021). The *Rht-D1b* dwarfing allele was the major QTL for TKW and in KIN18 had a positive effect on SpS. Photoperiod insensitivity gene *Ppd-D1a* decreased SpS in both environments. Previously identified earliness variants on chromosomes 3A and 5A (*Qncb.HD-3A*, *Qncb.HD-5A*) were colocated with QTL for fewer SpS, and a variant in *Vrn-A3* affecting heading date is colocated with a QTL for TKW on the short arm of chromosome 7A.

Recently characterized variants in wheat genes *Tb-B1*, *B-A1*, *WAPO-A1*, and *TaGW-A2* were predicted to segregate based on KASP marker genotypes of the parents (Supplementary Table 1). Yield component QTL were mapped near each of these genes. For example, predictive marker for the *B-A1* locus determining presence or absence of awns on the spike was the peak marker for TKW and SpS on the long arm of chromosome 5A (Table 1). In addition, a predictive marker for *Lr9* conferring resistance to leaf rust (caused by *Puccinia triticina*) was significant also for both TKW and SpS at KIN18, where plants were affected by a naturally occurring leaf rust epidemic. Beyond these known variants, QTL affecting SpS were identified on chromosomes 2A, 2B, 3D, and 6D, and a QTL on chromosome 7A was identified for TKW (Table 1).

Of the 20 QTLs, 7 were significant in both locations (Table 1); however, the relative proportion of additive genetic variation associated with QTL varied between locations (Fig. 3). No individual QTL increased both SpS and TKW, but in some, the magnitude of the negative effect on one phenotype was much smaller than the magnitude of the positive effect on the other.

Network mapping of yield component QTL using SEM

During 2019, data were collected for correlated morphometric traits KpS, KL, and KW in addition to SpS and TKW (Supplementary Fig. 1). Considering the analysis of the yield components in 2018, a SEM was fit that utilized PH and heading date in each environment to control for effect of plant growth genes on SY and allowed QTL to alter multiple yield component traits pleiotropically. In KIN19 and GA19, where leaf rust was observed and individual plots scored for disease severity, leaf rust score was added in as an additional variable. The network mapping model identified 53 QTLs in KIN19 (Supplementary Fig. 2 and Fig. 4), 62 QTLs in RAL19, and 57 QTLs in GA19 (Supplementary File 2). In this model, QTL for TKW and SpS colocated with PH or heading date loci were generally not detected. The exceptions were *Rht-D1* and *Ppd-D1*, suggesting they may have both direct

and indirect effects on yield components. All other QTL identified for TKW and SpS in 2018 were identified by the model at one or more locations in 2019.

Path analysis of phenotypes

Correlations between phenotypes may arise due to underlying genes with pleiotropic effects, linkage between loci, or causal relationships between traits. The correlation between heading date and PH was insignificant ($P > 0.05$) after including the effects of QTL affecting both traits, implying that the correlation of unadjusted phenotypes resulted from pleiotropic effects or close linkage between underlying genes (i.e. *Ppd-D1* and *Rht8*). Compensation is often observed in wheat, resulting in negative correlations between base yield component phenotypes KL, KW, KpS, and SpS. While these negative correlations can arise due to pleiotropic effects of the underlying genes, they may also result from source limitations. For example, in an environment or genetic background where carbohydrate availability limits grain yield, increasing the number of spikelets per spike may decrease the numbers of kernels per spikelets, and increasing kernel number may reduce mean kernel size.

SEMs allow for the estimating the mediating effects and allow analysis of these relationships for individual loci. Loci identified by network mapping of QTL were fit in a full SEM for 2 locations where all developmental and yield component traits were evaluated (RAL19 and KIN19) to estimate phenotypic relationships after correcting for direct QTL effects (Fig. 5). As yield component traits are plastic at different developmental stages, only effects of base yield component traits on subsequently developing traits were estimated. For example, increasing SpS may decrease kernel size but not vice versa, as spikelet number is set prior to grain fill. As kernel density was not directly measured in this experiment, plant growth phenotypes and mapped QTL were allowed to affect TKW directly.

Generally positive relationships of similar effect were observed between kernel measurements (KL, KW, TKW) and SY in both environments, with larger kernels contributing positively to SY, particularly at KIN19 (Fig. 5). As expected, KN and TKW individually had strong positive relationships with their respective component traits. Comparison of the estimated graphs indicated differences in the relationships between developmental traits and base yield components at each environment. At RAL19, there was little evidence for source limitation, although a slight negative effect of increasing spikelets per spike on KW was observed. In comparison, the KIN19 environment appeared more source-limited, with negative relationships between SpS and KpS, and strong negative effects of increasing kernel number on kernel size components KL and KW (Fig. 5). Consistent with the understood physiology of spike development, increasing heading date increased the number of spikelets per spike in both locations. Later heading was also associated with increased KW at RAL19. However, a slight decrease in KW was observed at KIN19 where plants experienced higher temperatures during grain fill (Supplementary Table 2). In addition, decreasing PH was associated with increasing KpS at KIN19. These effects were consistent with the appearance of source constraints in Kinston as suggested by the negative relationships between base yield components. Increased leaf rust severity (RS) decreased TKW and KL, but had a slightly positive effect on KpS. In general, lower overall SY in Kinston than in Raleigh along with the negative relationships between yield components suggests that source limitations at this location change the effect of QTL on SY (Supplementary Table 2). These source limitations may be produced in part from

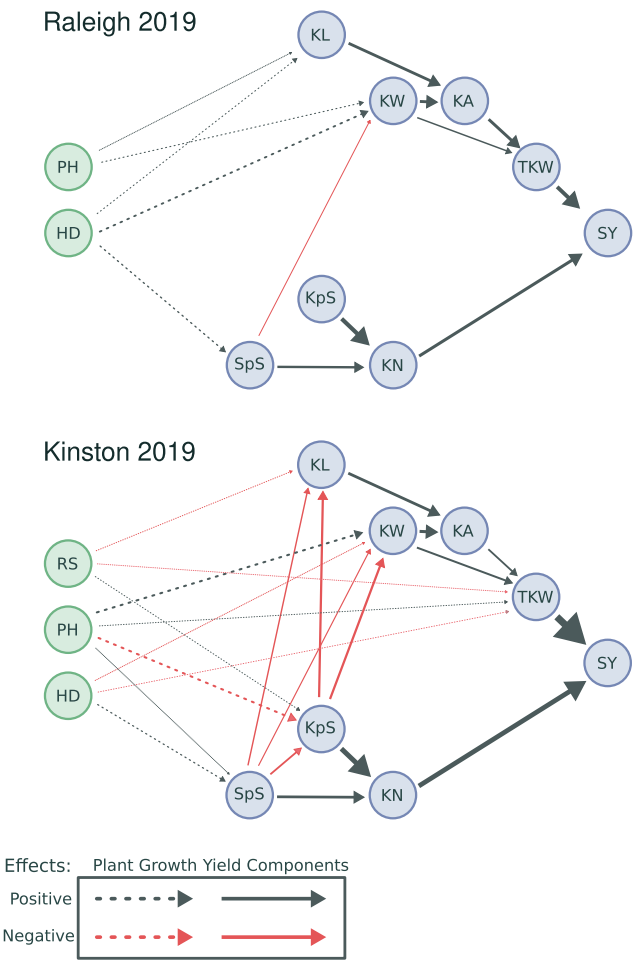

Fig. 5. Phenotype graph for Raleigh and Kinston 2019. Interphenotype coefficients for full SEM model (including QTL effects which are not shown) fit in Raleigh and Kinston 2019. Thickness of paths demonstrates standardized effect size, while color indicates direction of effect. Leaf rust score (RS) is shown in Kinston but not Raleigh, where no pathogen affected plants. Negative correlations between yield components in Kinston after correcting for genetic effects suggest environment-specific source constraints.

greater abiotic stress in the form of decreased precipitation and increased temperatures during grain fill, or from greater biotic stress in the form of increased leaf rust incidence. Taken together, this analysis indicates that variability in relationships among phenotypes across environments provided a mechanism for QTL to have environment specific effects on SY, even while having consistent direct effects on the primary phenotype.

Genetic architecture of SY

Additive genetic variation in SY and its components was largely associated with identified QTL, but the relative importance of those QTL varied from across environments (Fig. 6). A control test of 100 iterations was performed where the markers used to construct the yield component and plant growth relationship matrices were populated with random markers instead of genotypes for identified QTL. In these iterations these randomly sampled covariance matrices did not capture any variance, suggesting that the matrices constructed from mapped QTL are meaningful and not just recreating genome-wide covariance between individuals. The QTL with the overall largest contribution to additive genetic variation was *Rht-D1*. At RAL19 and GA19, *Rht-D1* was

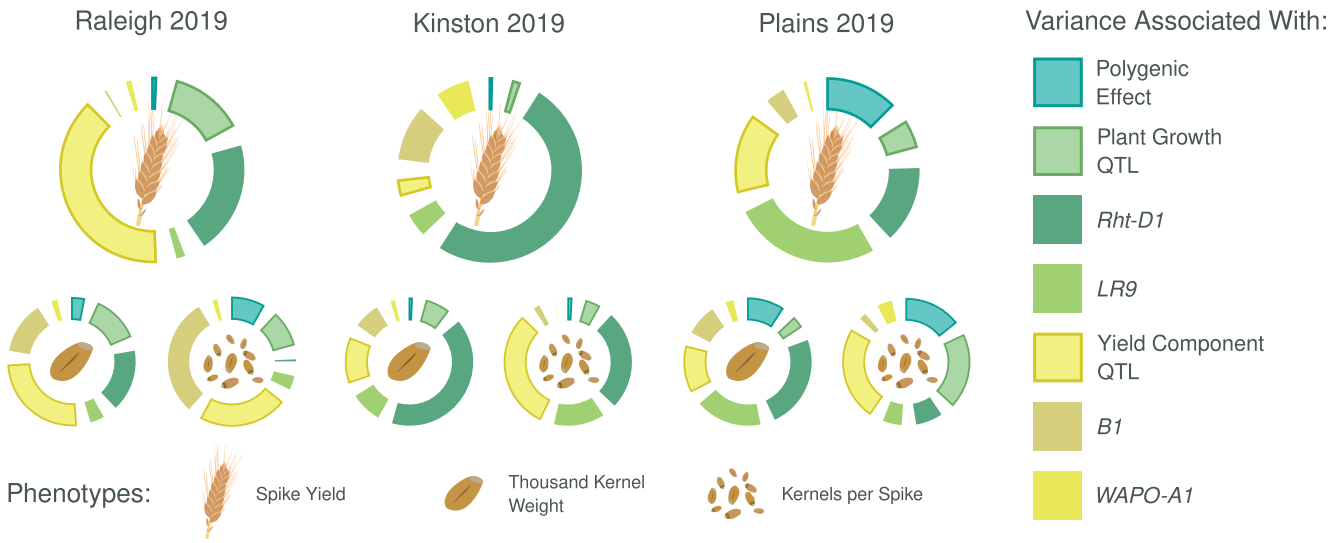

Fig. 6. Spike yield additive genetic variance components. Partitioning of additive genetic variance associated with different subsets of marker genotypes in all 3 locations (Raleigh 2019, RAL19; Kinston 2019, KIN19; Plains 2019, GA19). The genetic architecture of spike yield changes dramatically from environment to environment, with a relationship to the genetic architecture of component traits TKW and KN.

associated with 18.2% of additive genetic variation in SY, being primarily associated with TKW and explaining little additive genetic variation in KN. In contrast, at KIN19 *Rht-D1* was associated with 54.6% of additive genetic variation for TKW and 34.0% for KN, and 67.7% of additive genetic variation in SY. This is consistent with the large effect of PH on both KW and KpS at KIN19 observed in the path analysis (Fig. 5).

Resistance gene *Lr9* showed a pattern of environment-specific expression consistent with the presence of disease. Leaf rust pressure was highest at GA19 where *Lr9* was associated with 34.8% of additive genetic variation in SY, moderate at KIN19 where *Lr9* was associated with 5.6% of variation, and absent at RAL19 where the locus explained 1.6% of variation.

None of the per se yield components had effects comparable to *Rht-D1* on SY in any location and relative importance of other loci varied. All yield QTL together explained more than a third of additive genetic variation in SY at RAL19. Although *B1* explained a substantial portion of additive genetic variation in negatively correlated traits TKW and KN in this environment, it was associated with almost no additive genetic variation in SY. The *B1* awn suppressor explained a substantial proportion of additive genetic variation for SY at GA19 and KIN19, but very little for KN (Fig. 6). Interestingly, *WAPO-A1* was associated with 8.0% of additive genetic variation for SY at KIN19 and almost no additive genetic variation for SY at RAL19 and GA19. The differential importance of QTL in different environments suggests that the magnitudes of QTL effects on SY change from environment to environment through both differential effects on the yield components themselves and altered relationships between yield components.

The small proportion of additive genetic variation associated with the polygenic background across environments validates the ability of the mapping model to identify the loci generating yield component variation within each environment. The polygenic effect was largest at GA19, explaining over 15% of variation, but less than 5% at RAL19 and KIN19. The combined contribution of all other identified plant growth and yield component QTL was small for GA19 and KIN19. In contrast, at RAL19 2.7% of the additive genetic variance was associated with these yield component QTL, and 15.7% with plant growth QTL.

Consistent with the association of most additive genetic variation for SY with identified QTL, explicit consideration of mapped QTL improved prediction accuracies for overall SY substantially. Cross-validation prediction accuracies for SY increased slightly in all 3 environments when using a Bayesian LASSO model designed to accommodate QTL of large effects compared to a standard GBLUP model (Supplementary Table 3). Compared to the Bayesian LASSO model fit with all effects, a Bayesian LASSO model fit with only marker information on the plant growth and yield component QTL improved prediction accuracies substantially (from 0.27 to 0.39 in RAL19, from 0.28 to 0.59 in KIN19, and from 0.29 to 0.51 in GA19). This result suggests that the SEM mapping model which accounts for traits that affect the trait of interest improve power to detect markers important for trait prediction.

Major PH and heading date allele effects

Differences in the relative importance of individual loci and categories of loci were examined in-depth using path analysis in the full network model. *Rht-D1* explained a substantial portion of additive genetic variation in all environments but dominated total additive genetic variation in KIN19. To understand the mechanism by which the *Rht-D1* effect differed between RAL19 and KIN19, predicted allele effects on SY were estimated via path analysis starting with the estimated QTL effects of *Rht-D1* in both environments (Fig. 7). In both environments, the LA-95135 *Rht-D1b* allele has a slight positive effect on heading date, but strong negative effects on PH and KW. *Rht-D1b* reduces growth by preventing the degradation of the DELLA protein it alters, rendering plants insensitive to gibberellic acid (Peng *et al.* 1999). This affects the growth of cells in developing kernels and the elongating stem tissue, which may lead to direct effects on both PH and KW (Keyes *et al.* 1990). *Rht-D1b* was associated with an increase in heading date in both environments, contributing to slight increases in SpS and KN. Reduced PH due to *Rht-D1b* at KIN19 also contributed to increased KpS and further increased KN. In RAL19, a small negative effect of PH on KW resulted from the direct negative effect of *Rht-D1b* on this trait. In KIN19, a stronger association between PH and KW was observed along with a larger effect of *Rht-D1* on PH; decreased KW in this environment result

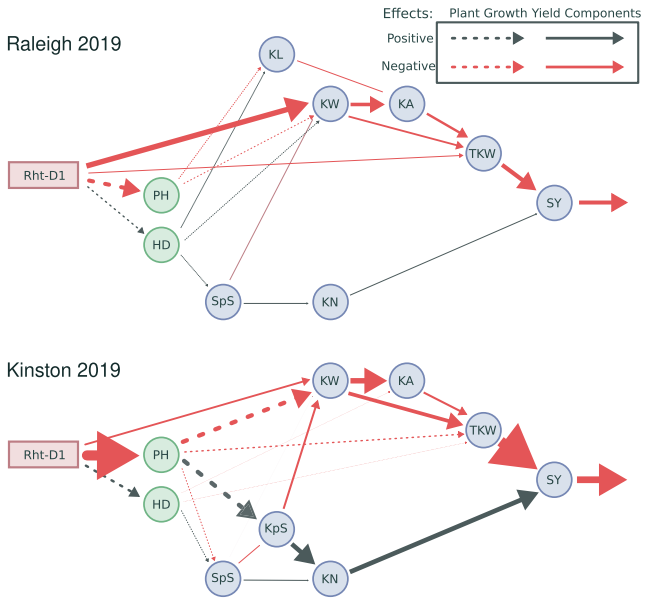

Fig. 7. Phenotype graph for *Rht-D1* allele effects. Interphenotype coefficients for full SEM model (including QTL effects which are not shown) fit in Raleigh and Kinston 2019. Colors and arrow size connecting component traits indicate the mediated effect of the LA-95135 allele (*Rht-D1b*) of the QTL on downstream phenotypes, not the path coefficients themselves. Thickness of paths demonstrates standardized effect size, while color indicates direction of effect. Leaf rust score (RS) is shown in Kinston but not Raleigh, where no pathogen affected plants. Negative correlations between yield components in Kinston after correcting for genetic effects suggest environment-specific source constraints.

from both the direct effect of *Rht-D1b* and the indirect effect mediated by PH and KpS. While *Rht-D1b* was associated with decreased TKW in both environments, the effect in KIN19 was larger in part due to a stronger effect of PH on KW. In addition, the decrease in TKW had a larger negative effect on SY in KIN19 than in RAL19, so that *Rht-D1* explained a larger proportion of additive genetic variation in yield in the KIN19 environment. Thus, the specific *Rht-D1* by environment interactions were due to both differential effects of *Rht-D1* on PH and KW in the 2 environments, as well as different relationships between phenotypes in the 2 separate environments.

Major per se yield component allele effects

Allele coefficients and relationships between yield component phenotypes were used to investigate allele effects across the whole set of yield components in each environment (Fig. 8). While the direction of effects on base yield component phenotypes remains constant, effect sizes often change between environments. Additional changes in the effect from environment to the environment are produced by altered relationship between phenotypes. *B1* has a much larger estimated effect in KIN19 than in RAL19, tracking with its much greater importance for determining SY in that environment. At the same time, *B1* generates major variation in both TKW and KN in RAL19. The presence of awns is associated with increases in kernel weight and decreases in KN in both environments due to the positive effects on kernel density and length. At KIN19 the increase in kernel weight was larger than the decrease in KN, leading to a major positive effect on SY. However, at RAL19, the contrasting effects on component traits are similar and produce almost no SY effect. The presence of awns was also associated with a positive SY effect in GA19, with a smaller positive effect on TKW than in KIN19, but no negative effect on KN.

WAPO-A1, a recently identified gene involved in determining the number of spikelets per spike, was the largest per se QTL for SpS in the LM population. If *WAPO-A1* can consistently increase yield by increasing KN without altering kernel size, MAS may be used to increase yield by increasing the frequency of *WAPO-A1a* in breeding populations. However, the only environment where the increased SpS allele is associated with an increase in SY is GA19 (Fig. 8). The *WAPO-A1* allele from LA-95135 has a significant negative effect on SpS and is also associated with an increase in KpS and kernel density in RAL19 and KIN19, and an increase in KW in KIN19. An increase in kernel size associated with the decreased SpS allele also emerges because of the negative effect of SpS on KW in both environments. The effect at KIN19 on SY is greater, where decreasing SpS increases KpS, leading to a minor increase in both KN and a larger increase in kernel weight for the lower SpS allele. In our environments, the effect of decreasing SpS through *WAPO-A1* was small and was only associated with a decrease in yield in one environment. Increasing yield by increasing spikelet number through MAS for *WAPO-A1* will necessitate understanding the environmental conditions that lead to these altered relationships. The *TaGW-A2* gene is a negative grain size regulator. The LA-95135 allele of a SNP polymorphism in the promoter region segregating in the population was associated with an increase in SY at RAL19 and GA19 but a slight decrease at KIN19 (Fig. 8). In all environments, the LA-95135 allele is associated with increased TKW due to positive effects on KL and KW, and also with a decrease in KN. At RAL19 this decrease in KN resulted from a decrease in SpS, and at KIN19 with a decrease in KPS. In both cases, the decrease in KN is associated with an increase in TKW. The total negative effect of the increased KW allele on SY in KIN19 results from a relatively larger decreases in KN compared to the other 2 environments, where it is associated with an overall increase in SY.

The LA-95135 allele of a QTL mapped to the centromeric region of chromosome 3B is associated with decreases in both kernel size and SpS at RAL19 and GA19. The LA-95135 allele of *Qncb-3B* decreases KL and SpS in all environments, but is associated with increases in KpS at KIN19. This allele has a major negative effect on SY in RAL19 and GA19, as it decreased both TKW and KN. At KIN19, an increase in KpS contributed to a comparatively smaller negative effect on SY despite similar effects on KL and SpS. The QTL having effects in the same direction on both kernel size and number is further evidence that the pleiotropy observed for per se yield component QTL in this study is not arising solely from source constraints.

Qncb-3D is the major per se KL QTL in this population, increasing KL with smaller negative effects on KpS and SpS. In all environments, effects on SY are small and the QTL is associated with almost no additive genetic variation. Small positive or negative estimated effects of the allele result from contrasting positive effects on TKW and negative effects on KN.

Conclusions

Modeling the relationships between genotypes and phenotypes using SEM can help us understand the mechanisms behind observed marker–trait associations for yield, and their relative utility in marker-assisted selection. In all cases, the relative importance of a QTL in generating variation in SY relates to its predicted effect on SY as calculated by allele effects on base

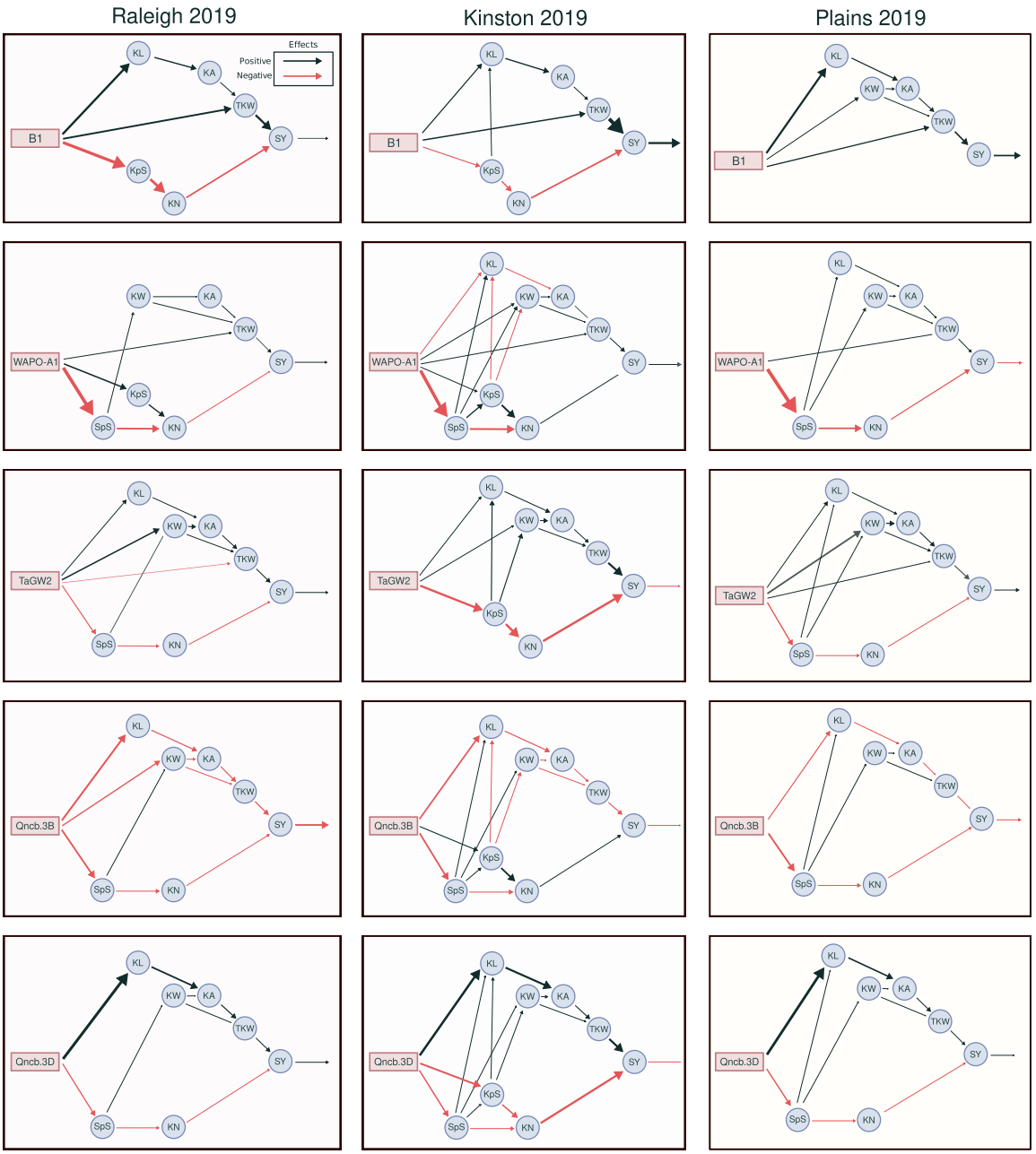

Fig. 8. LA-95135 allele effects of major yield component QTL. Models fit in each environment (columns; Raleigh 2019, RAL19; Kinston 2019, KIN19; Plains 2019, GA19) were used to estimate significant ($P < 0.10$) allele effects for previously mapped QTL on multiple base scaled yield component phenotypes, as well as effects on TKW presumed to be mediated by their effects on TW (kernel density). Effects of those allele effects on base phenotypes on additional phenotypes are estimated by path analysis using the estimated model, by the multiplication of the sum of effects on a phenotype by that phenotypes standardized effect on other phenotypes. Colors and arrow size connecting component traits indicate the mediated effect of the LA-95135 allele of the QTL on downstream phenotypes, not the path coefficients themselves. Many QTL generate substantial effects on yield components and little effect on spike yield, due to contrasting effects on component phenotypes. QTL effects vary significantly by environment, but only in magnitude and not in effect direction.

components and relationships between yield component phenotypes. Dissection of environment-specific SY effects demonstrates that variation in these effects emerges in part from altered allele effects on base yield components (most importantly, the presence or absence of an effect on a specific trait) as well as altered relationships between phenotypes in different environments. The different pleiotropic effects of major yield component QTL on base yield components suggests that these different QTL are affecting base yield components through different genetic pathways or physiological relationships. We observed a lower overall SY in KIN19 than in RAL19 that was associated with greater negative relationships between yield components in KIN19 relative to RAL19. This suggests that studying how physiological stresses limit source availability may provide insight into the altered effects of QTL on SY from environment to environment. In this study, a simple genetic structure and a large number of individuals was considered to attempt to limit overfitting and false-positives in the QTL mapping study. The application of these methods to more diverse material, including real-world breeding populations, requires further consideration and possibly

modifications to the model to account for population structure and differences in allele frequencies. RNA-sequencing and careful tracking of plant physiology in NILs contrasting for these major QTL may yield insights into how differences in sequence variation alter base yield components in environmentally specific ways.

We found no evidence in this study for the presence of QTL that consistently alter SY without altering plant phenology. Loci underlying heading date or PH may alter SY, because differences in heading date and PH generate differences in SY. The SY effect of heading date or PH QTL will then vary based on the relationship between these phenotypes and SY. Identified QTL are collectively associated with nearly all of the additive genetic variation in SY within each environment. However, the relative effects of QTL in each environment on SY, and therefore their relative contribution to yield variation, change in magnitude from environment to environment. Genomic selection models trained in these populations are then not averaging together QTL effects that vary from one location to the next due to error variation in effect estimates, but a combination of error variation and real differential expression of QTL. As the direction of QTL effects largely remained the same within these environments, these models still produce useful results—but suggests that there is room for improvement through an understanding and modeling of effect variation. There is no simple relationship between any identified QTL and SY. Additionally, while SY is an important component of overall grain yield, we expect the network of factors underlying yield to be even more complex. While this study used a large number of biparental lines in small plots to achieve high statistical power, application of these modeling techniques to larger yield plots in diverse material will present additional challenges. To truly make use of major genes in understanding and predicting yield, the underlying environmental factors altering differential QTL expression must be identified and explicitly modeled. SEM and network analyses similar to those utilized in this study may be one framework in which to do so.

Data availability

Genotype and phenotype data for the biparental population are available in supplemental files on (https://doi.org/10.25386/genetics.18282833). Code used to perform both standard QTL mapping and QTL mapping using SEM can be found on Github (https://github.com/noahddewitt/SEM_QTL).

Supplemental material is available at *GENETICS* online.

Acknowledgments

The authors thank staff of the USDA-ARS Plant Science Unit for assistance in genotyping and field evaluation of populations. Special thanks to Kim Howell, Kou Vang, and Jared Smith, who extracted DNA, prepared GBS libraries, and assisted with field work. Additional thanks to James B. Holland, Amanda Peters-Haugrud, Katherine Running, Meng Su, and Dylan Larkin, who all provided valuable feedback on early drafts of the manuscript.

Funding

Funding was provided by the Agriculture and Food Research Initiative Competitive Grants 67007-25939 (WheatCAP-IWYP) and 2022-68013-36439 (WheatCAP) from the USDA National Institute of Food and Agriculture. The funding body was not involved in the design of the study, the collection, analysis, and interpretation of data, or in the writing of the manuscript.

Conflicts of interest

None declared.

Literature cited

Addison CK, Mason RE, Brown-Guedira G, Guedira M, Hao Y, Miller RG, Subramanian N, Lozada DN, Acuna A, Arguello MN, *et al.* QTL and major genes influencing grain yield potential in soft red winter wheat adapted to the southern United States. Euphytica 2016; 209(3):665–677.

Boden SA, Cavanagh C, Cullis BR, Ramm K, Greenwood J, Jean Finnegan E, Trevaskis B, Swain SM. Ppd-1 is a key regulator of inflorescence architecture and paired spikelet development in wheat. Nat Plants. 2015;1(2):14016.

Borner A, Worland AJ, Plaschke J, Schumann E, Law CN. Pleiotropic effects of genes for reduced height (Rht) and day-length insensitivity (Ppd) on yield and its components for wheat grown in Middle Europe. Plant Breed. 1993;111(3):204–216.

Borrás L, Slafer GA, Otegui ME. Seed dry weight response to source-sink manipulations in wheat, maize and soybean: a quantitative reappraisal. Field Crops Res. 2004;86(2–3):131–146.

Brinton J, Uauy C. A reductionist approach to dissecting grain weight and yield in wheat. J Integr Plant Biol. 2019;61(3):337–358.

Broman KW, Wu H, Sen S, Churchill GA. R/qtl: QTL mapping in experimental crosses. Bioinformatics 2003;19(7):889–890.

Cheng X, Xin M, Xu R, Chen Z, Cai W, Chai L, Xu H, Jia L, Feng Z, Wang Z, *et al.* A single amino acid substitution in STKc_GSK3 kinase conferring semispherical grains and its implications for the origin of Triticumsphaerococcum. Plant Cell 2020;32(4):923–934.

Crespi BJ, Bookstein FL. A path-analytic model for the measurement of selection on morphology. Evolution 1989;43(1):18–28.

DeWitt N, Guedira M, Lauer E, Murphy JP, Marshall D, Mergoum M, Johnson J, Holland JB, Brown-Guedira G. Characterizing the oligogenic architecture of plant growth phenotypes informs genomic selection approaches in a common wheat population. BMC Genomics 2021;22(1):402.

DeWitt N, Guedira M, Lauer E, Sarinelli M, Tyagi P, Fu D, Hao Q, Murphy JP, Marshall D, Akhunova A, *et al.* Sequence-based mapping identifies a candidate transcription repressor underlying awn suppression at the B1 locus in wheat. New Phytol. 2020; 225(1):326–339.

Dhungana P, Eskridge KM, Baenziger PS, Campbell BT, Gill KS, Dweikat I. Analysis of genotype-by-environment interaction in wheat using a structural equation model and chromosome substitution lines. Crop Sci. 2007;47(2):477–484.

Fischer RA. The importance of grain or kernel number in wheat: a reply to Sinclair and Jamieson. Field Crops Res. 2008;105(1–2): 15–21.

Fischer RA, Quail KJ. The effect of major dwarfing genes on yield potential in spring wheats. Euphytica 1990;46(1):51–56.

Gilmour AR. Echidna Mixed Model Software. Journal of Agricultural, Biological, and Environmental Statistics 2018. https://doi.org/10.2307/1400446

Gilmour AR, Cullis BR, Verbyla AP, Verbyla AP. Accounting for natural and extraneous variation in the analysis of field experiments. J Agric Biol Environ Stat. 1997;2(3):269.

Grafius JE. A geometry for plant breeding. Crop Sci. 1964;4(3): 241–246.

Griffiths S, Wingen L, Pietragalla J, Garcia G, Hasan A, Miralles D, Calderini DF, Ankleshwaria JB, Waite ML, Simmonds J, *et al.* Genetic dissection of grain size and grain number trade-offs in CIMMYT wheat germplasm. PLoS One 2015;10(3):e0118847.

Isik F, Holland J, Maltecca C. Genetic Data Analysis for Plant and Animal Breeding. Cham: Springer International Publishing, 2017.

Kaplan RH, Phillips PC. Ecological and developmental context of natural selection: maternal effects and thermally induced plasticity in the frog *Bombina orientalis*. Technical Report 1. Evolution 2006. https://doi.org/10.1111/j.0014-3820.2006.tb01089.x

Keyes G, Sorrells ME, Setter TL. Gibberellic acid regulates cell wall extensibility in wheat (*Triticum aestivum* L.). Plant Physiol. 1990; 92(1):242–245.

Knott DR, Talukdar B. Increasing seed weight in wheat and its effect on yield, yield components, and quality. Crop Sci. 1971;11(2): 280–283.

Kuzay S, Xu Y, Zhang J, Katz A, Pearce S, Su Z, Fraser M, Anderson JA, Brown-Guedira G, DeWitt N, *et al.* Identification of a candidate gene for a QTL for spikelet number per spike on wheat chromosome arm 7AL by high-resolution genetic mapping. Theor Appl Genet. 2019;132(9):2689–2705.

Mi X, Eskridge K, Wang D, Baenziger PS, Campbell BT, Gill KS, Dweikat I. Bayesian mixture structural equation modelling in multiple-trait QTL mapping. Genet Res (Camb). 2010;92(3): 239–250.

Momen M, Ayatollahi Mehrgardi A, Amiri Roudbar M, Kranis A, Mercuri Pinto R, Valente BD, Morota G, Rosa GJM, Gianola D. Including phenotypic causal networks in genome-wide association studies using mixed effects structural equation models. Front Genet. 2018;9:455.

Momen M, Campbell MT, Walia H, Morota G. Utilizing trait networks and structural equation models as tools to interpret multi-trait genome-wide association studies. Plant Methods. 2019;15(1):107.

Nakagawa S, Schielzeth H. A general and simple method for obtaining R2 from generalized linear mixed-effects models. Methods Ecol Evol. 2013;4(2):133–142.

Peng J, Richards DE, Hartley NM, Murphy GP, Devos KM, Flintham JE, Beales J, Fish LJ, Worland AJ, Pelica F, *et al.* 'Green revolution' genes encode mutant gibberellin response modulators. Nature 1999;400(6741):256–261.

Sadras VO. 2007. Evolutionary aspects of the trade-off between seed size and number in crops. Field Crops Research 2007;100(2–3): 125–138.

Simons KJ, Fellers JP, Trick HN, Zhang Z, Tai YS, Gill BS, Faris JD. Molecular characterization of the major wheat domestication gene Q. Genetics 2006;172(1):547–555.

Su Z, Hao C, Wang L, Dong Y, Zhang X. Identification and development of a functional marker of TaGW2 associated with grain weight in bread wheat (*Triticum aestivum* L.). Theor Appl Genet. 2011;122(1):211–223.

Vargas M, Crossa J, Reynolds MP, Dhungana P, Eskridge KM. Structural equation modeling for studying genotype environment interactions of physiological traits affecting yield in wheat. J Agric Sci. 2007;145(02):151–161.

Wang W, Simmonds J, Pan Q, Davidson D, He F, Battal A, Akhunova A, Trick HN, Uauy C, Akhunov E. Gene editing and mutagenesis reveal inter-cultivar differences and additivity in the contribution of TaGW2 homoeologues to grain size and weight in wheat. Theor Appl Genet. 2018;131(11):2463–2475.

Wright S. The relative importance of heredity and environment in determining the piebald pattern of guinea-pigs. Proc Natl Acad Sci U S A. 1920;6(6):320–332.

Youssefian S, Kirby EJ, Gale MD. Pleiotropic effects of the GA-insensitive Rht dwarfing genes in wheat. 2. Effects on leaf, stem, ear and floret growth. Field Crops Res. 1992;28(3):191–210.

Ziyatdinov A, Vázquez-Santiago M, Brunel H, Martinez-Perez A, Aschard H, Soria JM. lme4qtl: linear mixed models with flexible covariance structure for genetic studies of related individuals. BMC Bioinformatics 2018;19(1):68.

Communicating editor: T. Juenger